Appl Biochem Biotechnol (2014) 172:176–187
DOI 10.1007/s12010-013-0528-0

# Characterization of a Layered Methylene Blue/Vanadium Oxide Nanocomposite and its Application in a Reagentless $H_2O_2$ Biosensor

**Xiaobo Zhang · Dan Li · Fujun Yin · Junyan Gong · Xujie Yang · Zhiwei Tong · Xingyou Xu**

Received: 26 June 2013 / Accepted: 15 September 2013 /
Published online: 21 September 2013


**Abstract** Layered nanocomposite of methylene blue (MB)-intercalated vanadium oxide was obtained through a simple hydrothermal synthesis method using MB, $V_2O_5$, and NaI as starting materials. The intercalation reaction was proven to be successful using X-ray diffraction pattern. The MB-$V_2O_5$ nanocomposite was characterized using a scanning electron micrograph, infrared spectra, thermogravimetric analysis, UV spectra, and electrochemical measurements. The intercalated MB cations showed a fine diffusion-controlled electrochemical redox process and facilitated the immobilized horseradish peroxidase's (HRP) good catalytic reduction upon $H_2O_2$. The as-prepared MB-$V_2O_5$/HRP biosensor showed a linear response to $H_2O_2$ over a range from $2.0\times10^{-6}$ to $9.5\times10^{-5}$ M with a detection limit of $9.7\times10^{-7}$ M (S/N ratio=3).

**Keywords** Methylene blue · Intercalation · Vanadium oxide · Horseradish peroxidase · Hydrogen peroxide biosensor

X. Zhang · D. Li · F. Yin · J. Gong · Z. Tong
Department of Chemical Engineering, Huaihai Institute of Technology, Lianyungang 222005, People's Republic of China

X. Zhang · F. Yin · X. Yang · X. Xu
Key Laboratory of Soft Chemistry and Functional Materials, Ministry of Education, Nanjing University of Science and Technology, Nanjing 210094, People's Republic of China

Z. Tong (✉)
SORST, Japan Science and Technology Agency (JST), Kawaguchi Center Building 4-1-8, Kawaguchi-shi, Saitama 332-0012, Japan
e-mail: zhiweitong575@hotmail.com

X. Xu
School of Life Science and Chemical Engineering, Huaiyin Institute of Technology, Huai'an 223003, People's Republic of China

## Introduction

Intercalation compounds are a unique type of materials, in which the mobile guest species are intercalated into a crystalline host lattice that has an interconnected system of an empty lattice site of appropriate size. What is interesting is that after intercalation, the structural integrity of the host lattice is still retained, and the host–guest interaction usually endows the intercalates with prominent properties such as catalysis [1], photocatalysis [2], photoresponse [3], electrooxidation [4], and photoluminescent [5, 6] and electroconductive [7] behaviors. Various host materials have been found to undergo such intercalation reactions, among which the layered metal oxides have attracted many interests. Vanadium pentoxide ($V_2O_5$) is a typical layered metal oxide semiconductor with an orthorhombic crystalline structure which can be utilized as intercalation compound. In the two-dimensional structure of $V_2O_5$, each layer consists of $VO_5$ square pyramids that share edges and corners. The vanadium atoms form a very short V–O bond with the apical oxygen and four much longer bonds with the basal oxygen [8]. It is the anisotropy of this layered structure that gives rise to the ability to insert guest species in perovskite-like cavities [9].

A large variety of organic guest species intercalated into $V_2O_5$ has been reported, including polyaniline [7, 10–12], polypyrrole [12], porphyrin [13], $[Co(phen)_3]^{2+}$ [14], amines [15, 16], and viologens [17, 18]. The obtained nanocomposites have found applications especially in electrochromism and electrochemistry. However, traditional ion exchange method seldom succeeds in preparing ion-intercalated composites of $V_2O_5$ because of the electric neutrality nature of its layers. Nevertheless, if the host layers of $V_2O_5$ can be partially reduced and become negatively charged, the intercalation of guest cations will be easily prepared through an electrostatic reaction between the host and the guest [19, 20].

Methylene blue (MB) is a typical basic dye with a plane structure being widely used as an electrochemical indicator [21, 22]; it can be immobilized with an electrode-modified material [23–25] or adsorbed on the surface of an electrochemical probe [26] for the detection of various reagents. Immobilization of MB with a polyion complex membrane has already been investigated, and catalytic reduction of $H_2O_2$ has been reported [27]. The kinetics of the intercalation of MB into $V_2O_5$ gels were reported by B Ackermans in 1996; however, the powder X-ray diffraction (XRD) spectrum of the intercalate was not given and the electrochemical properties of the hybrid have not been reported since then [28]. Our research group has succeeded in the intercalation of methylene blue into layered niobate [29] and titanoniobate [30]; the nanocomposites exhibit excellent electrochemical behaviors. In the present work, MB was intercalated into the interlayer of $V_2O_5$ through direct redox reaction of reducing agents $I^-$ and host $V_2O_5$ (Eq. 1). The laminar structure of MB-$V_2O_5$ nanocomposite was proven using XRD data, scanning electron micrograph (SEM), infrared (IR) spectra, thermogravimetric analysis (TGA), and UV spectra. The electrochemical behaviors of the MB-$V_2O_5$ hybrid thin film were studied, the nanocomposite was utilized with immobilization of enzyme (horseradish peroxidase (HRP)) to construct a $H_2O_2$ biosensor, and the MB-$V_2O_5$/HRP biosensor showed fast response and good reproducibility.

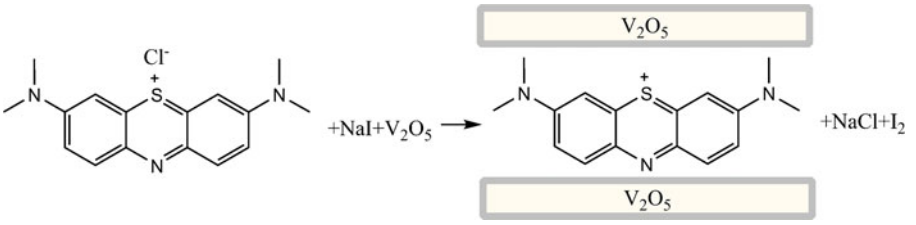

## Experimental Details

### Reagents

Analytical $V_2O_5$, NaI, and $H_2O_2$ (30 % (*w*/*v*) solution) were purchased from Sinopharm Chemical Reagent Co. Ltd., MB was purchased from Alfa Asia, and horseradish peroxidase (250 U $mg^{-1}$) was purchased from Shanghai Yuanye Biotechnology Co. Ltd.; all reagents were used without further purification.

### Apparatus

XRD patterns were collected with a M21X (MAC Co., Ltd.) diffractometer (monochromatic Cu Kα radiation, λ=0.15406 nm) at 30 kV and 30 mA with 2θ going from 3° to 70° in 1° steps. SEM images were taken with a JSM-6390 apparatus (JEOL) for the Au-coated sample. UV absorption spectra were carried out using a UV–vis spectrometer (UV-2550). IR spectra were measured on a Nicolet Impact 410 FT-IR spectrometer with the use of KBr pellets. Thermogravimetry (TG) and differential scanning calorimetry (DSC) were carried out on a Shimadzu DTG-60 apparatus at a heating rate of 20 °C $min^{-1}$ from room temperature to 600 °C in air. Electrochemical experiments were investigated in a conventional three-electrode electrochemical cell connected to a CHI 660C electrochemical workstation at room temperature, with a platinum electrode as counter electrode, a saturated calomel electrode (SCE) as reference electrode, and the modified electrode as working electrode.

### Preparation of the MB-$V_2O_5$ Nanocomposite

The procedure for the preparation of the layered composite MB-$V_2O_5$ was described as follows: a 1.9:1:1 molar ratio mixture of $V_2O_5$, MB, and NaI powder was dissolved in 10 mL of deionized water and stirred vigorously at room temperature for 5 h; the color of the mixture changed from yellow to dark blue. The solution was then transferred into a Teflon-lined stainless autoclave and heated at 120 °C for 8 h to obtain a dark green powder. After hydrothermal reaction, the resulting mixture was washed with deionized water and alcohol and centrifuged repeatedly until the supernate became colorless. The precipitate was at last dried in a vacuum oven at 60 °C for 12 h to obtain the nanostructured composite MB-$V_2O_5$.

### Preparation of the Modified Electrode

The nanocomposite-modified electrode was prepared as follows: 2 mg of MB-$V_2O_5$ was dispersed in 2 mL of ultrapure water to form a dark green suspension, and then 6 μL of the suspension was cast on the surface of a glass carbon electrode (GCE) and dried at room temperature. The acting electrolyte was 0.1 mol $L^{-1}$ of phosphate-buffered saline (PBS; pH= 7.0) solution. The solution was bubbled with $N_2$ for 20 min before examination in order to avoid the influence of oxygen.

To prepare MB-$V_2O_5$/HRP biosensor, 6 μL of HRP solution (10 mg of HRP and 2 mg of chitosan in 1-mL ultrapure water) was cast on the MB-$V_2O_5$-modified electrode and dried at 4 °C for at least 24 h. The enzyme electrode was rinsed with PBS thoroughly prior to use. A study of the effect of pH on the electrochemical behavior of the biosensor was carried out beforehand, and the optimum pH value was 7.0, so all the electrocatalytic studies were performed in $N_2$ saturated PBS (pH=7.0) solution at a scan rate of 50 mV $s^{-1}$. A $2\times10^{-3}$ M $H_2O_2$ solution was used for the successive dropping of $H_2O_2$ in the test.

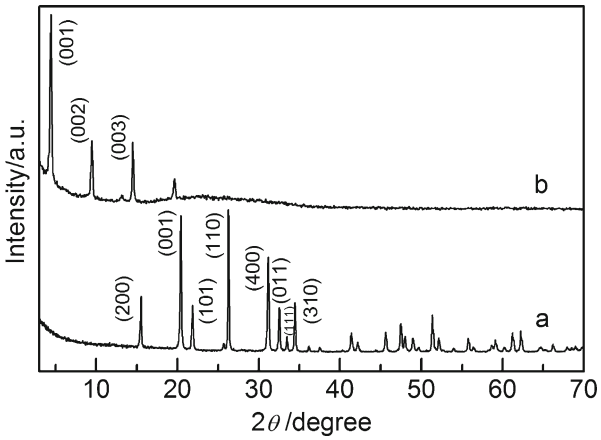


**Fig. 1** The X-ray diffraction patterns of (**a**) $V_2O_5$ powder and (**b**) MB-$V_2O_5$ thin film

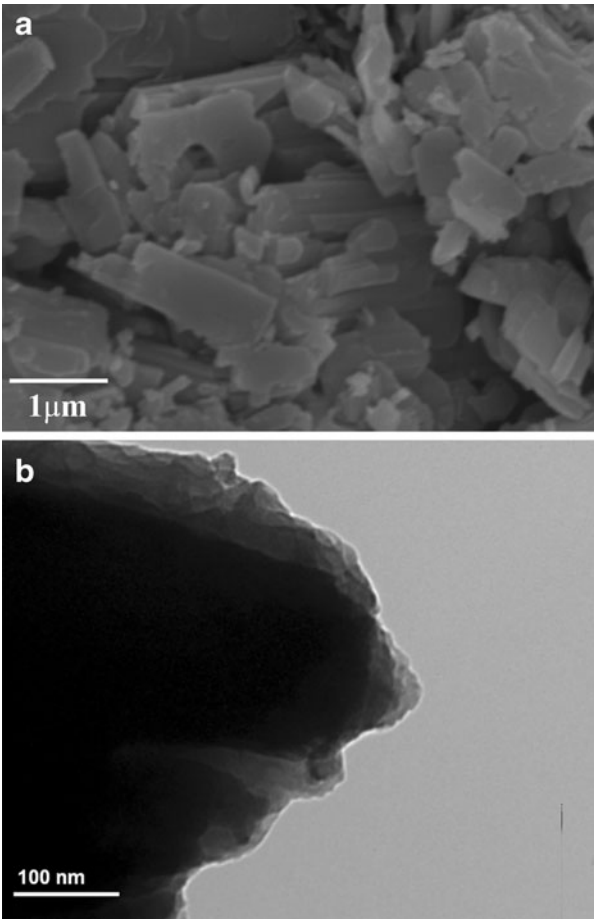


**Fig. 2** **a** SEM graph of $V_2O_5$ powder and **b** TEM graph of MB-$V_2O_5$ nanocomposite

## Results and Discussion

### Characterization of MB-$V_2O_5$ Nanocomposite

The layered structures of $V_2O_5$ powder and MB-$V_2O_5$ nanocomposite were identified by XRD analysis, which is shown in Fig. 1. The layer structure of the $V_2O_5$ host before intercalation (Fig. 1a) is in good agreement with the standard data (JCPDS 41–1426) for orthorhombic $V_2O_5$ [31, 32], and the sharp peaks in Fig. 1b indicates that the MB-$V_2O_5$ nanocomposite possesses a well-ordered lamellar structure and maintains good crystallinity after the intercalation [15]. The XRD pattern of the $V_2O_5$ powder in Fig. 1a shows a $d_{001}$ spacing of 0.44 nm, which is consistent with those of other references [9, 33]; the peak with the highest intensity at the low-diffraction angle in Fig. 1b reflects that the $d_{001}$ spacing of MB-$V_2O_5$ nanocomposite increases to 2.0 nm, which confirms the intercalation of methylene blue into the inorganic layers of vanadium oxide [20, 34, 35]. The micromorphology of the MB-$V_2O_5$ nanocomposite in Fig. 2b shows that after the intercalation of MB, the aggregated laminar structure is retained [32].

According to [9], the distance between two single sheets of $V_2O_5$ making up the bilayer slab is approximately 0.29 nm; judging from the $d_{001}$ value of MB-$V_2O_5$ nanocomposite, the interlayer spacing of MB-$V_2O_5$ should be calculated as 2.0−0.29=1.71 nm. Considering the rectangular dimensions of MB molecules (1.70 nm×0.76 nm×0.325 nm) [36], we propose that the most possible models of $MB^+$ cation arrangement in the interlayer of $V_2O_5$ may be either a single layer with its 1.70-nm axis perpendicular to the $V_2O_5$ layer or a bilayer with its long axis parallel to the $V_2O_5$ layer, which is shown in Fig. 3.

The intercalation of MB into vanadium oxide was also confirmed using IR spectra in Fig. 4. The characteristic IR absorption peaks of MB in Fig. 4b [37–39] are located at 1,601 and 1,494 $cm^{-1}$ (stretching modes of the aromatic rings), 1,400 $cm^{-1}$ (C–N symmetric stretch), and 1,358 $cm^{-1}$ ($-CH_3$ symmetric deformation), while the absorption peaks of MB in MB-$V_2O_5$ moved to 1,598, 1,489, 1,391 and 1,339 $cm^{-1}$ (Fig. 4c) respectively, and we believe that the redshift of the absorption peaks is the consequence of the interaction between the host layer and the guest cation. In the spectrum of $V_2O_5$ powder (Fig. 4a), the band at 1,023 $cm^{-1}$ is ascribed to the stretching of the V=O group and bands at 825 and 594 $cm^{-1}$ are attributed to the vibrations associated with vanadium oxide bridges (V–O–V) [40]. As is shown in Fig. 4c, the characteristic absorption peaks of $V_2O_5$ are at 1,015, 801, and 565 $cm^{-1}$, respectively, with a redshift to lower the wave number by 8, 24, and 39 $cm^{-1}$. The shift of the peaks for the host layer towards a lower wave number indicates that the $V^{5+}$ in the host layers was partially reduced to $V^{4+}$; thus, the host layers are negatively charged and the electrostatic interaction of the host layer with the guest $MB^+$ cation may weaken the V=O and V–O–V bonds [16, 20, 40, 41]. Consequently, it can be concluded from the XRD and IR characterization that $MB^+$ has been intercalated into the interlayer spaces of $V_2O_5$ successfully without disturbing the structure of MB and the structural integrity of the host layer, and it can be estimated that the strong interaction that exists between the host layer and the guest MB may increase the thermal/electrochemical stability and the efficiency of photoinduced charge separation [42].

Figure 5 gives the TG–DSC curves of the MB-$V_2O_5$ nanocomposite. The first weight loss step from room temperature to 200 °C (1.7 %) is believed to be the vaporization of water, the second weight loss from 200 to 500 °C (43.4 %) indicates the decomposition of the intercalated MB, and the exothermic peaks at 314 and 470 °C can be ascribed to the loss of methyl groups and breakup of the aromatic ring, respectively. It is obvious that the thermostability of methylene blue greatly improved through its intercalation into the host interlayer of $V_2O_5$ [13, 20, 32].

UV–vis optical absorption of MB-$V_2O_5$ nanocomposite was investigated in comparison with the UV spectrum of the MB solution (0.5 m mol $L^{-1}$). Figure 6a shows that the $MB^+$ cation

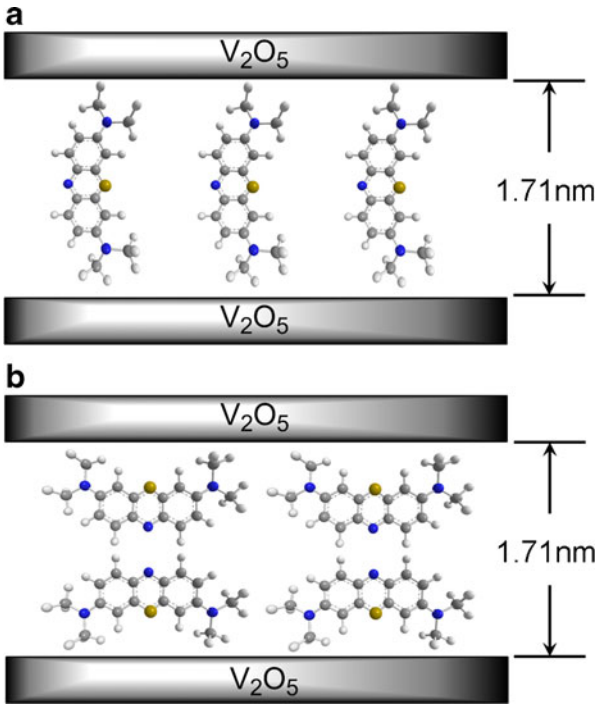


**Fig. 3** The proposed intercalation model of MB-$V_2O_5$: **a** single-layer vertical to $V_2O_5$ layer and **b** bilayer parallel to $V_2O_5$ layer

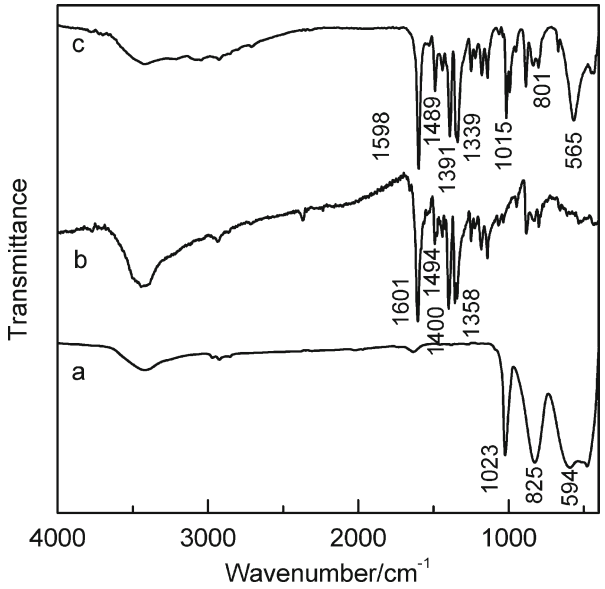


**Fig. 4** IR spectra of (**a**) $V_2O_5$, (**b**) MB, and (**c**) MB-$V_2O_5$ nanocomposites

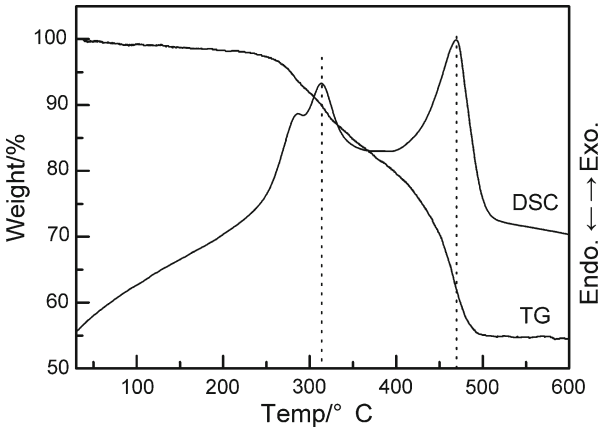


**Fig. 5** TG-DSC curves of MB-$V_2O_5$ nanocomposite

has a strong tendency to aggregate in aqueous solution and the typical maximum absorbance peaks are located at around 665 and 610 nm, ascribing to a monomer and dimer, respectively [37, 43]. The UV–vis spectrum of MB-$V_2O_5$ nanocomposite in Fig. 6b has a broad absorption band in the visible light region, presenting a maximum absorbance at 585 nm for the dimer and a shoulder at 695 nm for the monomer, which confirms the presence of MB in the nanocomposite. It can be deduced from the UV spectra that the intercalation reaction begins with the reduction of MB by $V^{4+}$ species, followed by the formation of protonated MB (695 nm), and then the dimerization of the dye cation (585 nm), and this result coincides well with B. Ackermans' work [28]. The broad peak and highest UV absorbance of the MB-$V_2O_5$ nanocomposite at 585 nm clearly indicate that the $MB^+$ cations in $V_2O_5$ interlayer are mainly dimerized. The absorbance at 695 nm may be due to the methylene blue monomer absorbed on the surface of the nanocomposite.

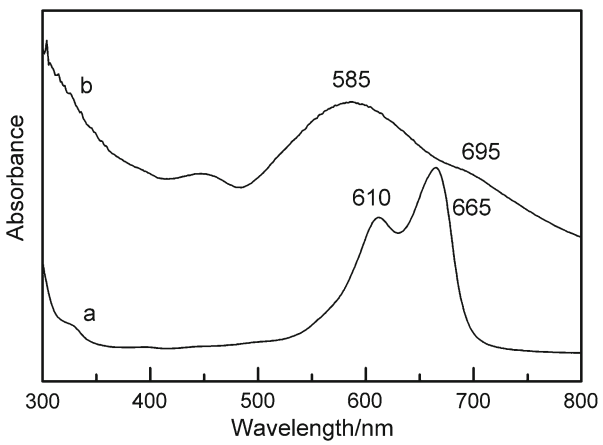


**Fig. 6** UV spectrum of MB in aqueous solution (0.5 m mol $L^{-1}$) (**a**) and MB-$V_2O_5$ nanocomposites (**b**)

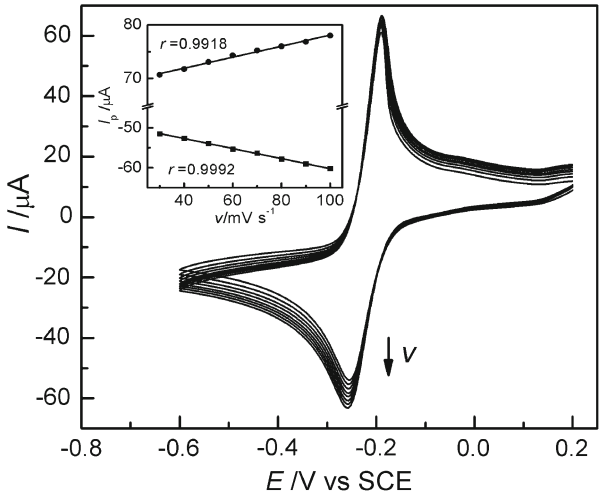


**Fig. 7** CVs of MB-$V_2O_5$ thin film at different scan rates (30, 40, 50, 60, 70, 80, 90, and 100 mV $s^{-1}$ from inner to outer) in 0.1 mol $L^{-1}$ PBS solution (pH=7.0). Insert: $I_c$~υ curve for MB-$V_2O_5$ nanocomposite thin film in 0.1 mol $L^{-1}$ PBS solution (pH=7.0)

## Electrochemical Behavior of MB-$V_2O_5$ Nanocomposite Thin Film

The CV curves of MB-$V_2O_5$ nanocomposite thin film on GCE in 0.1 mol $L^{-1}$ PBS (pH=7.0) at scan rates from 10 to 100 mV $s^{-1}$ are shown in Fig. 7. There are a couple of sensitive oxidation/reduction peaks indicating the two-electron transfer reaction of MB cations [23, 44]. Take the curve at a scan rate of 50 mV $s^{-1}$ for example: the redox potentials are at −0.257 and −0.190 V with a peak separation of 67 mV, which is enlarged by the immobilization of the dye cations in the host interlayer [30, 45]. As the scan rate increases from 10 to 100 mV $s^{-1}$, both $E_{pc}$

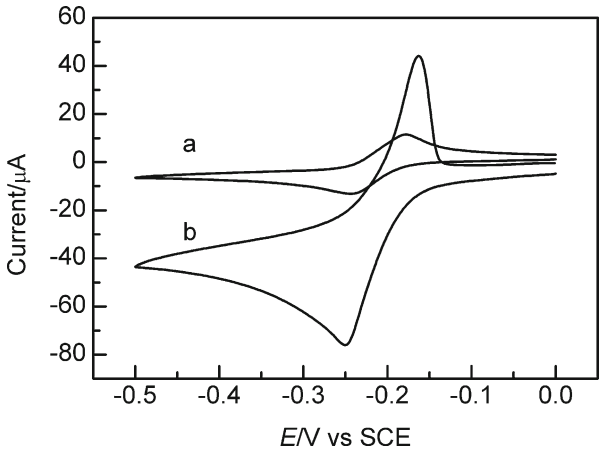


**Fig. 8** Cyclic voltammograms of MB-$V_2O_5$/HRP electrode in the absence of $H_2O_2$ (**a**) and at the presence of $5.83\times10^{-5}$ M $H_2O_2$ (**b**) in 0.1 mol $L^{-1}$ PBS solution (pH=7.0) at scan rate of 50 mV $s^{-1}$

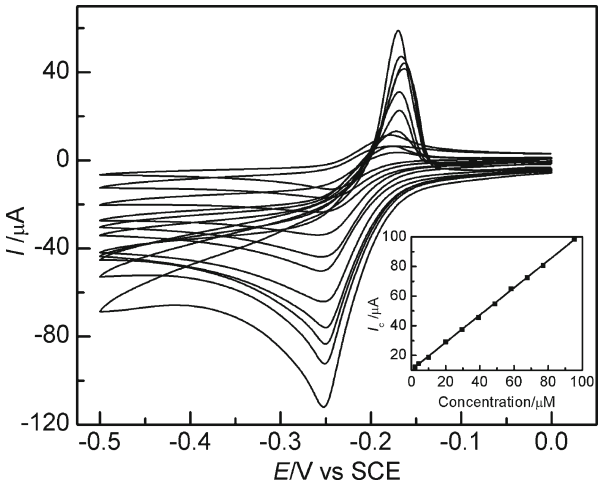


**Fig. 9** Cyclic voltammograms of MB-$V_2O_5$/HRP electrode in 0.1 M PBS (pH=7.0) solution at different concentrations of $H_2O_2$, that is, with 10, 20, 50, 100, 150, 200, 250, 300, 350, 400, and 500 μL of $2\times10^{-3}$ M $H_2O_2$ solution into 10 mL PBS from inner to outer. Scan rate is 50 mV $s^{-1}$. Insert: calibration curve between the cathodic peak current and the concentration of $H_2O_2$

and $E_{pa}$ change a little and $\Delta E_p$ remains stable, indicating a reversible electron transfer process of the $MB^+$ cations in the interlayer space at low scan rates. The peak currents ($I_c$ and $I_a$) are in perfect direct proportion with the scan rates (Fig. 7 insert), suggesting that the oxidation–reduction behavior of $MB^+$ in the $V_2O_5$ interlayer is controlled by the surface reaction.

In order to test the electrochemical stability of the MB-$V_2O_5$ hybrid film, the modified GCE was tested for 20 repeated cycles at scan rate of 50 mV $s^{-1}$. The cyclic voltammetric curves remain stable after the repeated cycles, with almost no observable changes in both the peak current and the peak separation, which confirms that the layers of $V_2O_5$ effectively stabilize the $MB^+$ cations. With excellent electrochemical stability and reproducibility of the nanocomposite enhanced by the intercalation reaction, the MB-$V_2O_5$ hybrid material will find practical applications in electroanalytical chemistry.

## Characterization of the MB-$V_2O_5$/HRP $H_2O_2$ Biosensor

Figure 8 shows the cyclic voltammetric behaviors of the MB-$V_2O_5$/HRP electrode with and without the existence of $H_2O_2$. It can be seen in Fig. 8a that the redox behavior of the intercalated MB cation retained with the immobilization of HRP; however, the peak currents decreased as a result of the influence of HRP and the inertness of chitosan in the film. When $H_2O_2$ was added, both the reduction and oxidation peak currents increased and the cathodic peak potential shifted towards the negative direction, which demonstrated that MB can mediate the electron transfer between HRP and GCE and facilitate the bioactivity of the enzyme towards reduction of $H_2O_2$.

The reaction mechanism of the biosensor can be proposed according to the literature [27, 38, 46]:

- HRP reduced hydrogen peroxide to water:

$$H_2O_2 + HRP \rightarrow H_2O + HRP\text{–I}$$

- HRP then was regenerated by the intercalated methylene blue through two separate one-electron steps:

$$HRP\text{–I} + (MB\text{–}V_2O_5)_{red} \rightarrow HRP\text{–}II + (MB\text{–}V_2O_5)_{ox}$$

$$HRP\text{–}II + (MB\text{–}V_2O_5)_{red} \rightarrow HRP + (MB\text{–}V_2O_5)_{ox}$$

$$(MB\text{–}V_2O_5)_{ox} + 2e \rightarrow (MB\text{–}V_2O_5)_{red}$$

The intercalated MB underwent oxidation during the regeneration of HRP, which can be seen from the increase of the oxidation peak current. MB can then be recycled through reduction reaction at the electrode, which endows the MB-$V_2O_5$/HRP biosensor good stability and reproducibility; therefore, the reduction current increased proportionally to the concentration of $H_2O_2$ in the PBS solution.

The electrochemical catalytic reduction behaviors of the MB-$V_2O_5$/HRP electrode on $H_2O_2$ at different pH were studied, and the hybrid shows the best catalytic behavior at pH 7.0 of the PBS at a scan rate of 50 mV $s^{-1}$. An excellent linear relationship of the cathodic peak current $I_{pc}$ to $H_2O_2$ concentration $c$ ranging from $2.0\times10^{-6}$ to $9.5\times10^{-5}$ M was obtained, as was shown in Fig. 9. The linear relationship can be given as $I_{pc}$ (μA)=0.9198$c$ (μM)+10.4382 ($r$=0.9995, $n$=11); a detection limit of $9.7\times10^{-7}$ M was obtained with a signal-to-noise ratio of 3. The above biosensor has a lower detection limit than the biosensor that is based on the immobilization of HRP on DNA–silver nanohybrids and PDDA-protected gold nanoparticles constructed by Ma, and it is also easy to prepare [47]. The stability of the biosensor was studied by successive tests in $1.0\times10^{-5}$ M $H_2O_2$ solution every day for 20 times; the obtained RSD was 1.15 %, which indicated good stability of the biosensor towards detection of $H_2O_2$. To the best of our knowledge, the interaction between HRP and intercalated MB with layered $V_2O_5$ was investigated for the first time. It is obvious that the $V_2O_5$ host layer plays an important role in the mediation activity of MB, and we believe that the MB-$V_2O_5$ nanocomposite has a potential application as a stable electron mediator in many electrocatalytic reactions.

## Conclusion

An electron mediator methylene blue intercalated layered $V_2O_5$ was obtained through a simple redox process. The MB-$V_2O_5$ nanocomposite has been characterized using XRD, SEM, IR spectra, TGA, and UV spectra, and the electrochemical properties have been investigated. It was confirmed that the intercalated $MB^+$ cations are mainly aggregated in the form of dimers. Electrochemical studies indicated that the interaction between the host layer and the guest dye cation enhanced the electrochemical stability of the nanocomposite. The as-prepared nanocomposite was immobilized with HRP to construct an enzyme biosensor for the detection of $H_2O_2$, and the as-prepared biosensor possessed good sensitivity and stability. It can be concluded that the nanocomposite can be utilized as an excellent mediator, and other electrochemical applications are being investigated in our laboratory.

**Acknowledgments** This work was supported by Natural Science Fund of Jiangsu Province (BK2012665), Key University Science Research Project of Jiangsu Province (11KJA430008), and Jiangsu Marine Resource

Development Research Institute Foundation (JSIMR10E06). This work is also funded by the Priority Academic Program Development of Jiangsu Higher Education Institutions and Natural Science Foundation (Huaihai Institute of Technology, China, no. 2010150013).

## References

1. Centi, G., & Perathoner, S. (2008). *Microporous and Mesoporous Materials, 107*, 3–15.
2. Lin, H.-Y., Lee, T.-H., & Sie, C.-Y. (2008). *International Journal of Hydrogen Energy, 33*, 4055–4063.
3. Tong, Z., Takagi, S., Tachibana, H., Takagi, K., & Inoue, H. (2005). *Journal of Physical Chemistry B, 109*, 21612–21617.
4. Forti, J. C., Manzo-Robledo, A., Kokoh, K. B., de Andrade, A. R., & Alonso-Vante, N. (2006). *Electrochimica Acta, 51*, 2800–2808.
5. Matsumoto, Y., Unal, U., Kimura, Y., Ohashi, S., & Izawa, K. (2005). *Journal of Physical Chemistry B, 109*, 12748–12754.
6. Kudo, A., & Sakata, T. (1996). *Journal of Physical Chemistry, 100*, 17323–17326.
7. Kanatzidis, M. G., Wu, C. G., Marcy, H. O., & Kannewurf, C. R. (1989). *Journal of the American Chemical Society, 111*, 4139–4141.
8. Seong, S., Yee, K. A., & Albright, T. A. (1993). *Journal of the American Chemical Society, 115*, 1981–1987.
9. Wang, Y., & Cao, G. (2006). *Chemistry of Materials, 18*, 2787–2804.
10. Wu, C. G., DeGroot, D. C., Marcy, H. O., Schindler, J. L., Kannewurf, C. R., Liu, Y. J., et al. (1996). *Chemistry of Materials, 8*, 1992–2004.
11. Li, Z. F., & Ruckenstein, E. (2002). *Langmuir, 18*, 6956–6961.
12. Huguenin, F., & Torresi, R. M. (2008). *Journal of Physical Chemistry C, 112*, 2202–2209.
13. Anaissi, F. J., Engelmann, F. M., Araki, K., & Toma, H. E. (2003). *Solid State Sciences, 5*, 621–628.
14. Lu, Y., Wang, E., Chen, J., Qi, Y., Hu, C., Xu, L., et al. (2004). *Journal of Solid State Chemistry, 177*, 946–950.
15. Kweon, H., Lee, K. W., & Lee, C. E. (2010). *Current Applied Physics, 10*, 1152–1155.
16. Chen, W. (2004). *Materials Letters, 58*, 2275–2278.
17. Kato, I., Nakato, T., Kuroda, K., & Kato, C. (1990). *Colloids and Surfaces, 49*, 241–245.
18. Nakato, T., Kato, I., Kuroda, K., & Kato, C. (1989). *Journal of Colloid and Interface Science, 133*, 447–451.
19. Bose, A., He, P., Liu, C., Ellman, B. D., Twieg, R. J., & Huang, S. D. (2001). *Journal of the American Chemical Society, 124*, 4–5.
20. Kong, A., Ding, Y. J., Wang, P., Zhang, H. Q., Yang, F., & Shan, Y. K. (2011). *Journal of Solid State Chemistry, 184*, 331–336.
21. Liu, S., Wang, L., & Zhao, F. (2007). *Journal of Electroanalytical Chemistry, 602*, 55–60.
22. Yin, Y., Zhang, H., & Nishinari, K. (2007). *Journal of Physical Chemistry B, 111*, 1590–1596.
23. Chen, H.-Y., Ju, H.-X., & Xun, Y.-G. (1994). *Analytical Chemistry, 66*, 4538–4542.
24. Zhang, J., Zheng, Y., Jiang, G., Yang, C., & Oyama, M. (2008). *Electrochemistry Communications, 10*, 1038–1040.
25. Zhu, H., & Zhao, G.-C. (2009). *Microchimica Acta, 165*, 329–334.
26. Wang, J., Wang, F., & Dong, S. (2009). *Journal of Electroanalytical Chemistry, 626*, 1–5.
27. Gu, T., & Hasebe, Y. (2004). *Analytica Chimica Acta, 525*, 191–198.
28. Ackermans, B., Schoonheydt, R. A., & Ruiz-Hitzky, E. (1996). *Journal of the Chemical Society, Faraday Transactions, 92*, 4479–4484.
29. Zhang, X., Feng, D., Chen, M., Ding, Z., & Tong, Z. (2009). *Journal of Materials Science, 44*, 3020–3025.
30. Zhang, X., Liu, C., Liu, L., Zhang, D., Zhang, T., Xu, X., et al. (2010). *Journal of Materials Science, 45*, 1604–1609.
31. Zoubi, M., Farag, H., & Endres, F. (2009). *Journal of Materials Science, 44*, 1363–1373.
32. Quites, F. J., Bisio, C., RdCG, V., Landers, R., Marchese, L., & Pastore, H. O. (2012). *Journal of Colloid and Interface Science, 368*, 462–469.
33. Kuwahara, T., Tagaya, H., & Kadokawa, J. (2001). *Inorganic Chemistry Communications, 4*, 63–65.
34. Malta, M., Louarn, G., Errien, N., & Torresi, R. M. (2003). *Electrochemistry Communications, 5*, 1011–1015.
35. O'Dwyer, C., Navas, D., Lavayen, V., Benavente, E., Santa Ana, M. A., González, G., et al. (2006). *Chemistry of Materials, 18*, 3016–3022.
36. Klika, Z., Čapková, P., Horáková, P., Valášková, M., Malý, P., Macháň, R., et al. (2007). *Journal of Colloid and Interface Science, 311*, 14–23.
37. Gutiérrez-Tauste, D., Domènech, X., Casañ-Pastor, N., & Ayllón, J. A. (2007). *Journal of Photochemistry and Photobiology, A187*, 45–52.

38. Yao, H., Li, N., Xu, S., Xu, J. Z., Zhu, J. J., & Chen, H. Y. (2005). *Biosensors and Bioelectronics, 21*, 372–377.
39. Yan, Y., Zhang, M., Gong, K., Su, L., Guo, Z., & Mao, L. (2005). *Chemistry of Materials, 17*, 3457–3463.
40. Lee, J. M., Hwang, H.-S., Cho, W.-I., Cho, B.-W., & Kim, K. Y. (2004). *Journal of Power Sources, 136*, 122–131.
41. Grigorieva, A. V., Goodilin, E. A., Anikina, A. V., IV, & Kolesnik, Y. D. T. (2008). *Mendeleev Communications, 18*, 71–72.
42. Zhu, D., Liu, H., Lv, L., Yao, Y., & Yang, W. (2008). *Scripta Materialia, 59*, 642–645.
43. Ghanadzadeh, A., Zeini, A., Kashef, A., & Moghadam, M. (2008). *Journal of Molecular Liquids, 138*, 100–106.
44. SlHdA Nicolai, P. R. P., Rodrigues, S. M. L. A., & Rubim, J. C. (2002). *Journal of Electroanalytical Chemistry, 527*, 103–111.
45. Xian, Y., Liu, F., Xian, Y., Zhou, Y., & Jin, L. (2006). *Electrochimica Acta, 51*, 6527–6532.
46. Huang, R., & Hu, N. (2001). *Bioelectrochemistry, 54*, 75–81.
47. Ma, L., Yuan, R., Chai, Y., & Chen, S. (2009). *Journal of Molecular Catalysis B: Enzymatic, 56*, 215–220.